Structural Engineering and Mechanics, *Vol. 54, No. 3 (2015) 501-520*
DOI: http://dx.doi.org/10.12989/sem.2015.54.3.501

Effect of tension stiffening on the behaviour of square RC column under torsion

T. Ghosh Mondal[a] and S. Suriya Prakash*

Department of Civil Engineering, Indian Institute of Technology Hyderabad, India

(Received September 13, 2014, Revised December 10, 2014, Accepted January 13, 2015)

Abstract. Presence of torsional loadings can significantly affect the flow of internal forces and deformation capacity of reinforced concrete (RC) columns. It increases the possibility of brittle shear failure leading to catastrophic collapse of structural members. This necessitates accurate prediction of the torsional behaviour of RC members for their safe design. However, a review of previously published studies indicates that the torsional behaviour of RC members has not been studied in as much depth as the behaviour under flexure and shear in spite of its frequent occurrence in bridge columns. Very few analytical models are available to predict the response of RC members under torsional loads. Softened truss model (STM) developed in the University of Houston is one of them, which is widely used for this purpose. The present study shows that STM prediction is not sufficiently accurate particularly in the post cracking region when compared to test results. An improved analytical model for RC square columns subjected to torsion with and without axial compression is developed. Since concrete is weak in tension, its contribution to torsional capacity of RC members was neglected in the original STM. The present investigation revealed that, disregard to tensile strength of concrete is the main reason behind the discrepancies in the STM predictions. The existing STM is extended in this paper to include the effect of tension stiffening for better prediction of behaviour of square RC columns under torsion. Three different tension stiffening models comprising a linear, a quadratic and an exponential relationship have been considered in this study. The predictions of these models are validated through comparison with test data on local and global behaviour. It was observed that tension stiffening has significant influence on torsional behaviour of square RC members. The exponential and parabolic tension stiffening models were found to yield the most accurate predictions.

Keywords: square column; tension stiffening; softened truss model; torque; twist, compression

1. Introduction

The presence of torsional loading significantly alters the behaviour of reinforced concrete (RC) members. Although, a number of studies have addressed pure flexure, pure shear and pure torsion independently, investigations on such loads in combination are scarce. Among them, the combination of torsion and axial load is the least studied until now in spite of its occurrence in bridge columns. The presence of torsion loading is more likely in skewed or horizontally curved

∗Corresponding author, Assistant Professor, E-mail: suriyap@iith.ac.in
[a]Graduate Student, E-mail: ce13m1023@iith.ac.in

http://www.techno-press.org/?journal=sem&subpage=8 ISSN: 1225-4568 (Print), 1598-6217 (Online)

bridges, bridges with unequal spans or column heights, and bridges with outrigger bents. Construction of bridges with these configurations is often unavoidable due to site constraints. In addition, multidirectional earthquake motions (including significant vertical motions), structural constraints due to a stiff decking, movement of joints, abutment restraints, and soil conditions may also lead to combined load effects of torsion and axial compression in columns.

Given the brittle nature of torsional failure of RC members and high safety requirement for important buildings and bridges, it is essential to accurately predict the torsional behaviour of RC members for efficient design of these members. Though STM was developed to predict the torsional behaviour of reinforced concrete members, present investigation shows that STM prediction is not sufficiently accurate in the post cracking region when compared to test results. Therefore, the present study focuses on the development of improved analytical models for RC square columns subjected to torsion with and without axial compression. Since the concrete is weak in tension, its contribution to torsional capacity of RC members was neglected in the original STM. The present investigation revealed that, disregard to tensile strength of concrete is the main reason behind the discrepancies in the STM predictions. Similar observation was also found in a parallel study conducted on circular columns by Mondal and Prakash (2015). The existing STM is extended in this paper to include the effect of tension stiffening to get improved prediction of behaviour of square RC columns under torsion with and without axial compression. Three different tension stiffening models comprising a linear, a quadratic and an exponential relationship have been considered in this study. The predictions of the models are validated through comparison with test data on square RC columns under torsional loading.

2. Tension stiffening effect

Tension stiffening (TS) is explained with the simple case of a reinforced concrete member subjected to uniaxial tensile load as shown in Fig. 1. Concrete offers no resistance to applied tensile load at the cracked section and the entire load (P) is carried by steel alone (Fig. 1(a)). This makes the stress in concrete (σ_c) at the cracked locations equal to zero rendering maximum stress in the steel (f_S). At any section in between two adjacent cracks, where the concrete is intact, the applied load (P) is resisted together by steel (P_S) and concrete (P_C). With increase in distance from the crack locations, stress in concrete increases whereas the stress in steel (f_S) decreases (Fig. 1(b)). This leads to maximum stress in concrete and minimum stress in steel at the midpoint between two cracks. This phenomenon of considering tensile resistance offered by intact concrete in between the adjacent cracks is known as tension stiffening. As the load increases, crack formation continues until the cracks are so close that effective length of intact concrete between the cracks reduces to such a level that concrete is incapable of taking any more tensile stress perpendicular to the crack directions. At this stage, the concrete is considered to be completely cracked. Subsequently, the effect of tension stiffening becomes insignificant and inflicts no influence on the behaviour of RC members.

Under torsional loading, the shear flow created in an RC section due to the applied torsional moment can be resolved into a diagonal compression and a diagonal tension. When this diagonal tensile stress in an RC member reaches the tensile strength of concrete, cracks are developed. Even after torsional cracking, the concrete between the cracks contributes to load resistance. If this tension stiffening effect under torsion is disregarded, steel stresses are overestimated and as a result, structural safety could be underestimated considerably. Therefore, it is necessary that a

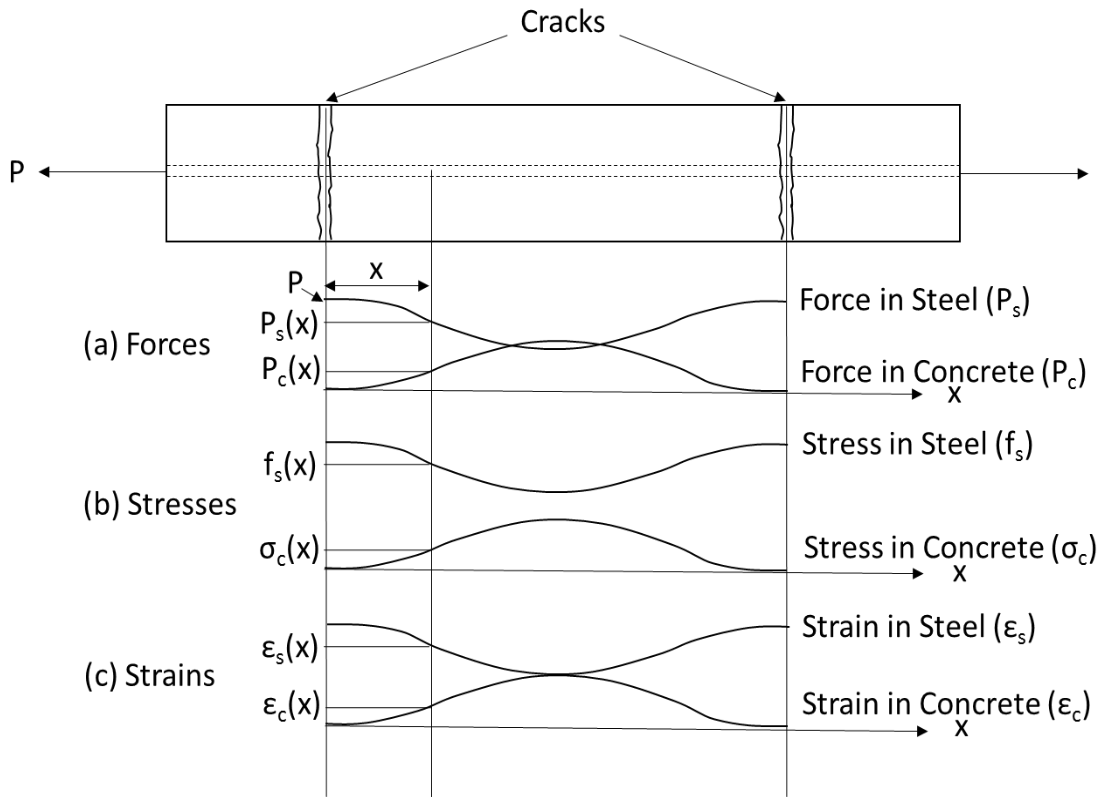

Fig. 1 Distribution of concrete stresses after cracking (Hsu 1993)

realistic STM model taking in to account the tension stiffening effect needs to be formulated for improved predictions. The present study shows the significance of tension stiffening through validation of tension stiffened STM predictions with experimental data on square RC columns tested under combined torsion and axial compression.

Several investigations (Choi and Cheung 1996, Elenas *et al*. 2006, Stramandinoli and Rovere 2008) in the past studied the influence of tension stiffening effect on the behaviour of RC members and different tension stiffening models were proposed. However, none of them were verified and validated with test data under torsional loading. Three models were proposed by Vecchio and Collins (1986), Belarbi and Hsu (1994), Stevens *et al*. (1987) for tension stiffening behaviour of concrete. However, they were empirical expressions developed using test data from 2-dimensional shear panels and do not closely model the 3-dimensional torsional response of RC members (Greene 2006). Hence, a modified set of equations, comprising a linear, a parabolic and an exponential relationship, were proposed by Greene (2006) based on regression analysis of torsional test data which are used in this investigation. The exponential model was earlier used by You and Belarbi (2011) under torsional load condition but was not verified with experimental data. The investigation by You and Belarbi focused on back-calculating the shear flow thickness based on the given experimental data. In the present work, the objective is to accurately predict the entire torque-twist behaviour by including tension stiffening relationships. All the three tension stiffening models (linear, parabolic and exponential) are verified with experimental data.

3. Tension-stiffened softened truss model

3.1 Background

This section describes the development of the existing Softened Truss Model (STM) (Hsu and Mo 1985a) by considering the effect of concrete tension stiffening (TS) for improved predictions. The inclusion of tension stiffening in the model is important because it allows an improved prediction of the service-level twist. A stress-strain relationship for concrete in tension was taken from literature (Greene 2006). The proposed TS-STM adopts the equilibrium and compatibility equations developed for an RC panel under a membrane stress field. The torsional moment and thickness of shear flow are given by Bredt's (1896) thin-tube theory. TS-STM model has not been validated well for columns under combined axial compression and torsion. The scope of present study includes validation of TS STM model with test data of RC square columns under torsion combined with and without axial compression.

3.2 Thickness of shear flow zone

An external torque applied to a reinforced concrete prismatic member is resisted by an internal torque formed by a circulatory shear along the periphery of the cross section (Fig. 2(a)). The shear stress distribution in a rectangular cross section due to the circulatory shear is shown in Fig. 2(c). It is zero at the centre of the section and increases linearly towards the edges. However, the variation is not linear along the diagonals. Along the diagonals, it is zero at the centre as well as at the corners and reaches a maximum somewhere in between. At the midway location on the sides of the section, shear stresses reach a maximum at the edges. In general, the shear stress values are more at the periphery of the section. Owing to such variation of shear stress, it can be stated that shear stress resisted by core of the section is small compared to that resisted by the outer part of the section. Thus, the shear flow q effectively occupies a zone, known as the shear flow zone towards the periphery of the section, and has a thickness denoted as t_d (Fig. 2). This thickness t_d is a variable determined from the equilibrium and compatibility conditions. It is not the same as the wall thickness h of a hollow member as shown in Fig. 2(c).

When an RC member is subjected to twist, the walls of the member are warped causing flexural stresses in the concrete struts. The original STM assumes that the shear flow zone is extended into the member up to the neutral axis. The concrete inside the neutral axis is in tension and considered ineffective. Such a member is assumed to be fully cracked, with the concrete and reinforcement acting as a truss. Previous research has shown this as an effective way to model a fully cracked RC member (Hsu and Mo 1985). However, it cannot reflect the torsional behaviour of an uncracked member. In the present study, the formulations are extended to predict the torsional behaviour of uncracked elements as well. Since the pre-cracking torsional behaviour of RC members under torsion is known to be linear, one can plot the variation of torque with twist before cracking from the cracking torsional moment and cracking twist values calculated from the expressions given by Collins and Mitchell (1991). Thickness of shear flow zone at cracking, t_{d0} can be calculated with the help of Eq. (1) (ACI 318 2005).

$$t_{d0} = \frac{3}{4}\frac{A_{cp}}{p_c} \tag{1}$$

In Eq. (1), p_c is the perimeter of the section and A_{cp} is the area of concrete bounded by p_c. The

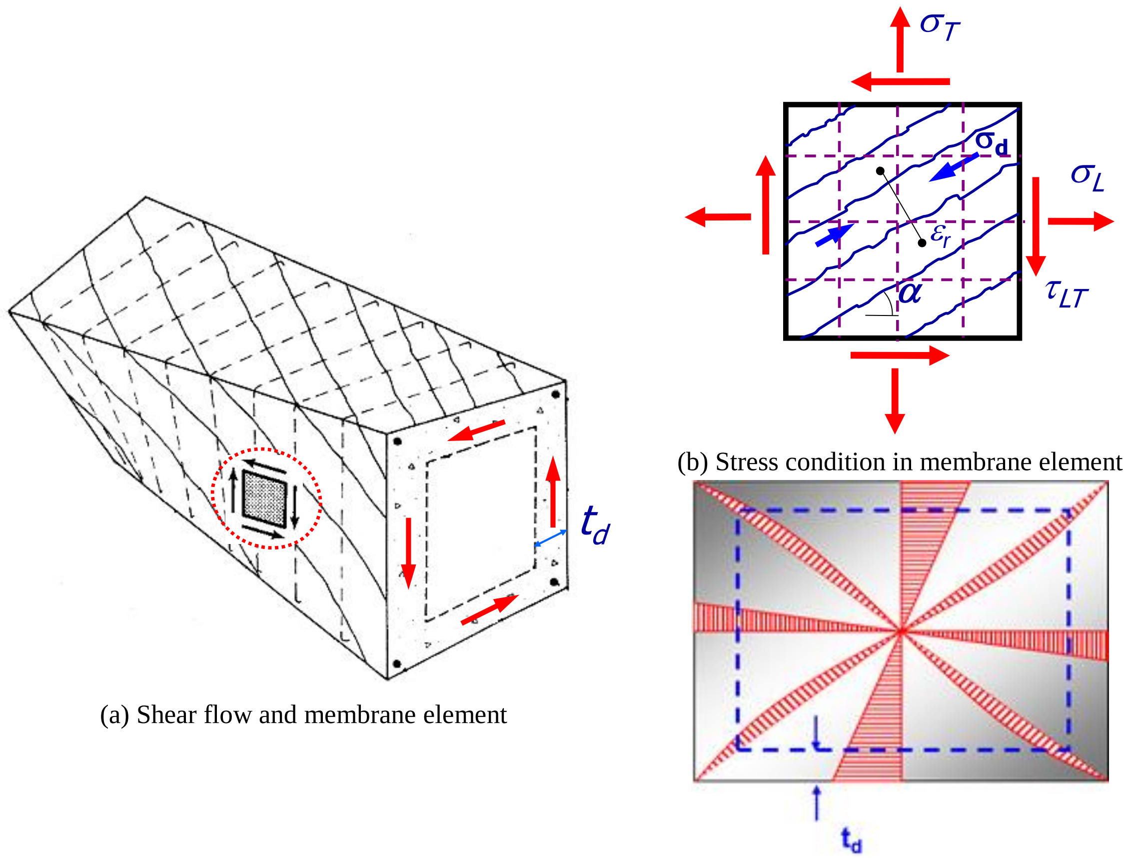

(a) Shear flow and membrane element

(b) Stress condition in membrane element

(c) Shear stress distribution in rectangular cross section

Fig. 2 Thickness of shear flow zone in prismatic members (Hsu 1993)

thickness of shear flow zone increases after cracking according to the increase in torsional moment till the peak point.

3.3 Shear element in shear flow zone

Fig. 2(b) shows stress condition in reinforced concrete membrane elements subjected to torsion without considering contribution from steel reinforcement. However, if steel reinforcement is also taken in to consideration, which is aligned in the *l* (longitudinal) and *t* (transverse) directions, the in-plane stress condition developed in the membrane element is as shown in Fig. 3. This forms the foundation of basic equilibrium equations under combined shear and normal stress condition. The total stress resisted by an RC element in the longitudinal (σ_l) and transverse (σ_t) directions can be broken into two components a) stress resisted by concrete, and b) stress resisted by steel reinforcement. The normal and shear stress resisted by concrete in the '*l*' and '*t*' directions can be expressed in terms of principal stresses σ_d and σ_l, which are oriented at an angle of α with the '*l*' and '*t*' axes respectively. After the development of diagonal cracks, the concrete struts are subjected to compression and the steel bars act as tension links, thus forming an apparent truss

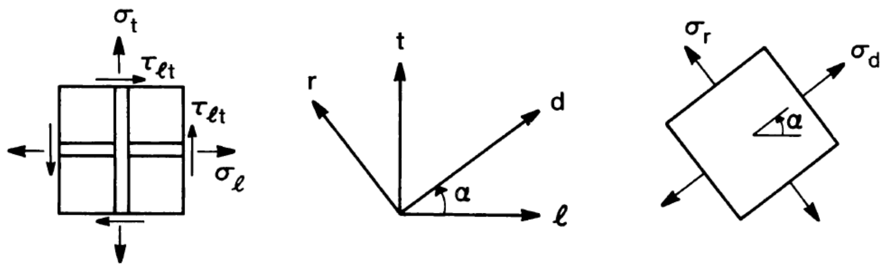

(a) Definitions of stresses and coordinate system

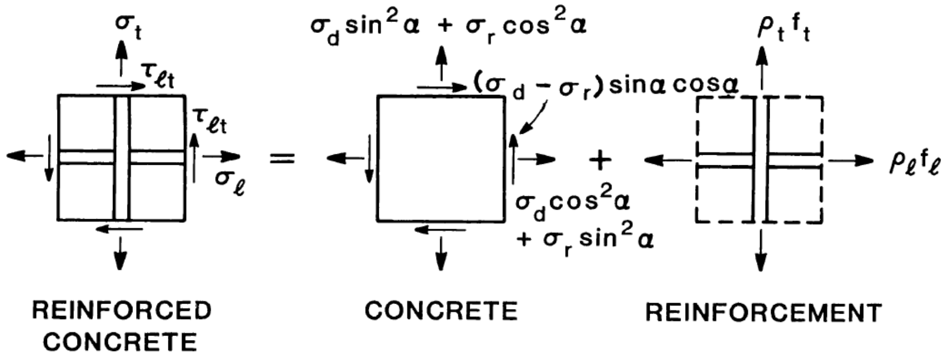

(b) Superposition of concrete stresses and steel stresses

Fig. 3 RC membrane element subjected to in-plane stresses (Adapted from Hsu 1988)

action. The compression struts are oriented along the d-axis, which is inclined at an angle α to the longitudinal direction. The normal principal stresses in the *d* and *r* directions are σ_d and σ_r respectively.

3.4 Governing equations in TS-STM

The proposed TS-STM adopts the equilibrium equations developed for an RC panel under a membrane stress field given by Eqs. (2)-(6). The torque, *T*, resisted by the section is given by Eq. (6) for a shear stress flowing around the perimeter of the section as described by Bredt's thin-tube theory (Bredt 1986). The compatibility relationships given by Eqs. (7)-(13), which describe the relationship between the unit twist, θ, and the shear strain, γ_{LT}, and the relationship between θ and the curvature in the concrete strut, ψ, respectively, are adopted without modification. Finally, constitutive relationships are used for the concrete and reinforcement as shown in Eqs. (14)-(22).

3.4.1 Equilibrium equations

The two dimensional equilibrium equations relate the average internal stresses developed in the concrete (σ_d and σ_r) and in the reinforcement (f_l and f_t) to the average applied stresses (σ_l, σ_t and τ_{lt}) with respect to the angle of inclination of d-axis to the l-axis, α. The torsional moment induced by internal shear stress can be expressed as Eq. (6).

$$\sigma_l = \sigma_d cos^2\alpha + \sigma_r sin^2\alpha + \rho_l f_l \tag{2}$$

$$\sigma_t = \sigma_d sin^2\alpha + \sigma_r cos^2\alpha + \rho_t f_t \tag{3}$$

$$\tau_{lt} = (-\sigma_d + \sigma_r) sin\alpha cos\alpha \tag{4}$$

$$\rho_l = \frac{A_l}{p_o t_d} \tag{5a}$$

$$\rho_t = \frac{A_t}{s t_d} \tag{5b}$$

$$T = \tau_{lt}(2A_0 t_d) \tag{6}$$

where ρ_l, ρ_t are volumetric ratios of longitudinal and transverse steel, $A_{l,}$ A_t are total cross-sectional areas of longitudinal and transverse steel and p_0, t_d are perimeter and the width of the shear flow zone respectively.

3.4.2 Compatibility equations

The two dimensional compatibility equations relate the average strains in $l - t$ co-ordinate system (ε_l, ε_t and γ_{lt}) to that (ε_d and ε_r) in $d - r$ co-ordinate system (principal axes). The compatibility equations are alone, not sufficient to solve the torsion problem. Infact additional equations that relate, the out of plane warping effects are necessary. The curvature of the concrete struts (ψ) can be related by geometry to the angle of twist (θ), angle of inclination (α), the thickness of shear flow zone (t_d) and the outer face strain of the concrete strut (ε_{ds}) as shown below.

$$\varepsilon_l = \varepsilon_d cos^2\alpha + \varepsilon_r sin^2 \tag{7}$$

$$\varepsilon_t = \varepsilon_d sin^2\alpha + \varepsilon_r cos^2\alpha \tag{8}$$

$$\frac{\gamma_{lt}}{2} = (-\varepsilon_d + \varepsilon_r) sin\alpha cos\alpha \tag{9}$$

$$\theta = \left({}^{p_o}/_{2A_o}\right)\gamma_{lt} \tag{10}$$

$$\psi = \theta sin2\alpha \tag{11}$$

$$t_d = {}^{\varepsilon_{ds}}/_{\psi} \tag{12}$$

$$\varepsilon_d = {}^{\varepsilon_{ds}}/_{2} \tag{13}$$

3.4.3 Constitutive laws

3.4.3.1 Concrete struts

An RC membrane element subjected to shear stresses is actually subjected to biaxial compression-tension stresses in the diagonal directions. Compressive strength in one direction is reduced by cracking due to tension in perpendicular direction. Vecchio and Collins (1981) incorporated this softening effect in the concrete stress – strain curve under compression and proposed the following relationships.

$$\sigma_d = k_1 \zeta f_c' \tag{14}$$

$$k_1 = \frac{\varepsilon_{ds}}{\zeta \varepsilon_o}\left(1 - \frac{\varepsilon_{ds}}{3\zeta \varepsilon_o}\right) \text{ for } \quad \frac{\varepsilon_{ds}}{\zeta \varepsilon_o} \leq 1 \tag{15a}$$

$$k_1 = \left[1 - \frac{\zeta^2}{(2-\zeta)^2}\right]\left(1 - \frac{\zeta \varepsilon_o}{3\varepsilon_{ds}}\right) + \frac{\zeta^2}{(2-\zeta)^2}\frac{\varepsilon_{ds}}{\zeta \varepsilon_o}\left(1 - \frac{\varepsilon_{ds}}{3\zeta \varepsilon_o}\right) \quad \text{for} \quad \frac{\varepsilon_{ds}}{\zeta \varepsilon_o} > 1 \tag{15b}$$

where, ζ is peak softening coefficient which is quantitatively a measure of diagonal tensile cracking of concrete. Hsu (1991) proposed the following expression for ζ in terms of diagonal tensile strain, ε_r.

$$\zeta = 0.9/\sqrt{(1 + 600\varepsilon_r)} \tag{16}$$

3.4.3.2 Concrete stress strain curves under tension

Models of tension stiffening are typically linear before cracking as shown in Eq. (17).

$$\sigma_r = E_s \varepsilon_r \tag{17}$$

After cracking, the tensile stress decreases rapidly with further increase in tensile strain. Previous equations for the descending branch were developed by Vecchio and Collins (1986), Belarbi and Hsu (1994), Stevens *et al*. (1987) which were empirical expressions developed using data from shear panels and do not closely model the data from torsional tests (Greene 2006). So, a modified set of equations, comprising a linear, a parabolic and an exponential relationship, proposed by Greene (2006) based on regression analysis of torsional test data are used in this study and are shown by Eqs. (18a), (18b) and (18c) respectively. The term β_r is a function of ε_r and is given by Eq. (20). The λ_t term in Eq. (18c) is a constant that controls the rate at which the function decays. The term ε_{cr0} in Eq. (20) is the strain at which the tensile stress intersects the strain axis. Also, the parabolic function is tangent to the stress axis at ε_{cr0}. The selected values of the constants (Green 2006) are summarised in Table 1. Normalized stress-strain data generated from the proposed equations are plotted and shown in Fig. 4.

$$\sigma_r = f_{cr}(1 - \beta_r) \tag{18a}$$

$$\sigma_r = f_{cr}(1 - 2\beta_r + \beta_r^2) \tag{18b}$$

$$\sigma_r = f_{cr}\, e^{-\lambda_t(\varepsilon_r - \varepsilon_{cr})} \tag{18c}$$

$$f_{cr} = C\frac{A_g}{A_{cp}}\sqrt{f_c'} \tag{19}$$

$$\beta_r = \frac{\varepsilon_r - \varepsilon_{cr}}{\varepsilon_{cr0} - \varepsilon_{cr}} \tag{20}$$

where ε_{cr} and f_{cr} are cracking strain and cracking stress respectively.

Table 1 Constants for average tensile stress (σ_r)

	C	ε_{cr0}	λ_t
Linear	0.500	0.00450	--
Parabolic	0.500	0.00700	--
Exponential	0.500	--	350

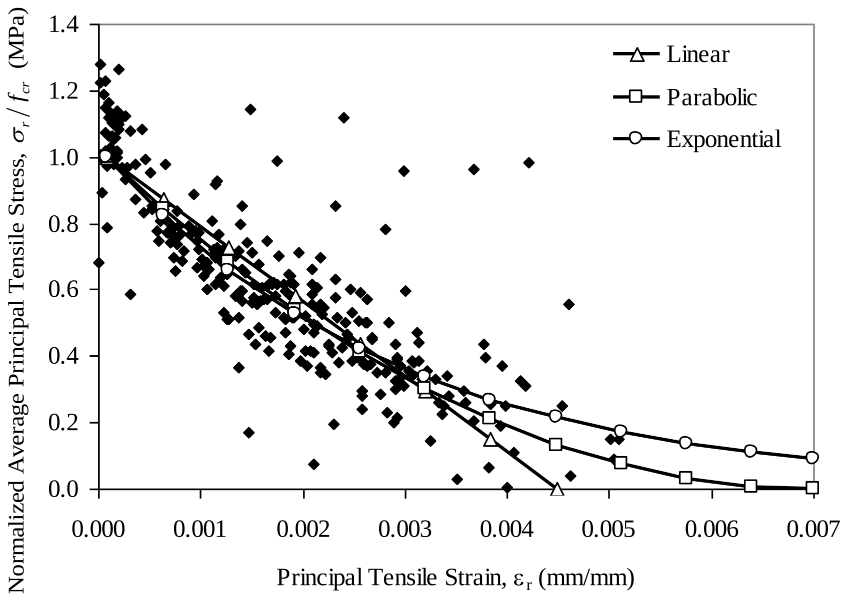

Fig. 4 Normalized data and tension stiffening relationships from literature (Greene 2006)
Note: ε_o was assumed to be -0.002 (Vecchio and Collins 1986).

3.4.3.3 Stress-strain relationship in mild steel

An elastic-perfectly plastic material model identical under tension and compression is assumed for steel reinforcements. The stress (f_l and f_t) in steel can be related to strain (ε_l and ε_t) before and after yielding as shown below.

For longitudinal steel

$$f_l = E_s \varepsilon_l \qquad \varepsilon_l < \varepsilon_{ly} \tag{21a}$$

$$f_l = f_{ly} \qquad \varepsilon_l \geq \varepsilon_{ly} \tag{21b}$$

For transverse steel

$$f_t = E_s \varepsilon_t \qquad \varepsilon_t < \varepsilon_{ty} \tag{22a}$$

$$f_t = f_{ty} \qquad \varepsilon_t \geq \varepsilon_{ty} \tag{22b}$$

Young's modulus of steel, E_s was assumed to be 200 GPa (ACI 318 2008). The yield strain of steel (ε_{ly} and ε_{ty} for longitudinal and transverse steel respectively) was calculated by dividing respective yield strength by E_s.

3.4.4 A_o and p_o

Area (A_0) enclosed by centre line of shear flow zone and the perimeter (p_o) of the enclosed area can be expressed as functions of t_d as shown below.

$$A_o = A_c - \frac{p_c t_d}{2} + t_d{}^2 \tag{23}$$

$$p_o = p_c - 4t_d \tag{24}$$

3.4.5 Expressions for ε_l and ε_t

The angle of inclination of diagonal struts to the member longitudinal axis of the member, α, is explicitly included in the equilibrium and compatibility equations. However, use of α can cause numerical instability in the iterative solution process. So, it was eliminated from the governing equations and the following relations were obtained.

$$\varepsilon_l = \varepsilon_d + \frac{A_o(-\varepsilon_d)(-\sigma_d+\sigma_r)}{-p_o\, t_d\,(\sigma_l-\sigma_r)+(A_l f_l)} \tag{25}$$

$$\varepsilon_t = \varepsilon_d + \frac{A_o s(-\varepsilon_d)(-\sigma_d+\sigma_r)}{p_o[-s\, t_d\,(\sigma_t-\sigma_r)+(A_t f_t)]} \tag{26}$$

The above equations can be solved simultaneously with the stress–strain relationships for steel.

3.4.6 Relations among strain components

From Eqs. (7) and (8), sin(α) and cos(α) can be estimated in terms of the strain components. Then making $\sin^2(\alpha)+\cos^2(\alpha)=1$, inter-relationship among the strain components can be obtained as shown in Eq. (27).

$$\varepsilon_r = \varepsilon_l + \varepsilon_t - \varepsilon_d \tag{27}$$

3.4.7 Angle of crack inclination (α)

From the estimated values of sin(α) and cos(α), angle of crack inclination (α) can be expressed in terms of strain components as shown in Eq. (28).

$$tan^2\alpha = \frac{\varepsilon_l-\varepsilon_d}{\varepsilon_t-\varepsilon_d} \tag{28}$$

Young modulus of concrete (E_c) can be calculated from cube compressive strength (f_{ck}) of concrete using the relation given in Eq. (29). The shear modulus (G) is related with Young modulus (E_c) and Poisson's ratio (γ) as shown in Eq. (30).

$$E_c = 5000\sqrt{f_{ck}} \quad \text{MPa} \tag{29}$$

where f_{ck} is cube compressive Strength of Concrete in MPa.

$$G = {E_c}/{(1+2\gamma)} \quad \text{MPa} \tag{30}$$

γ value was chosen to be equal to 0.2 for concrete.

3.4.8 Parameters at cracking

The expressions for estimation of parameters at cracking are tabulated in Table 2.

Table 2 Parameter to evaluate cracking torque and twist

Parameter	Expression
t_{cr}	${}^{3}/_{4}\,{}^{A_c}/_{p_c}$
GK	$G\dfrac{4A_o^2}{p_o}t$
T_{cr}	$\dfrac{A_c^2}{p_c}f_{cr}\sqrt{1+\dfrac{f_{pc}}{f_{cr}}}$
θ_{cr}	${}^{T_{cr}}/_{GK}$

GK is the torsional stiffness. t_{d0}, T_{cr} and θ_{cr} are the depth of shear flow zone, values of torque and twist at cracking respectively. A_c is the area enclosed by the outer perimeter of the concrete cross-section and p_c is the outer perimeter of concrete cross-section. f_{pc} is axial stress applied to the member.

4. Solution procedure

Given the dimensions of the cross section, the reinforcement, and the material properties, a 'displacement controlled' solution to the equations can be made by first selecting ε_d and then assuming trial values for ε_r and t_d. Next, an iterative procedure is used to find values of the assumed variables by solving the equilibrium equations, compatibility equations, and stress-strain relationships. This will find one point on torque-twist curve. The solution algorithm is explained in the Fig. 5. Subsequent points are found by varying the selected value of ε_d from a zero to maximum value that causes peak torque or that causes t_d to exceed a prescribed value. The indeterminacy in the equations is settled by putting $\sigma_l = constant$, $\sigma_t = 0$ and ε_r and t_d as variables.

A value of ε_d is selected and values of ε_r and t_d are assumed in an iterative manner. A loop is executed and all the equilibrium, compatibility and constitutive laws are satisfied and the unknown variables are found out. Then the calculated values of ε_r and t_d are compared with the assumed values and desired precision is arrived in an iterative manner. Thus a point on the torque-twist curve is traced. In this way, for every single ε_d value, corresponding ε_r and t_d values are obtained. As the ε_d reaches the maximum value, the loop is terminated and the torque-twist response is traced.

4.1 Initial calculations

The following initial calculations were made for variables that are constant during the solution process. Calculations of $\boldsymbol{A_c}$,$\boldsymbol{p_c}$, $\boldsymbol{t_{cr}}$, $\boldsymbol{f_{cr}}$, and $\boldsymbol{E_c}$ were done from the respective equations.

4.2 Solution algorithm

The following procedure was used to solve the proposed Square TS-STM. The algorithm is summarized as a flow chart in Fig. 5.

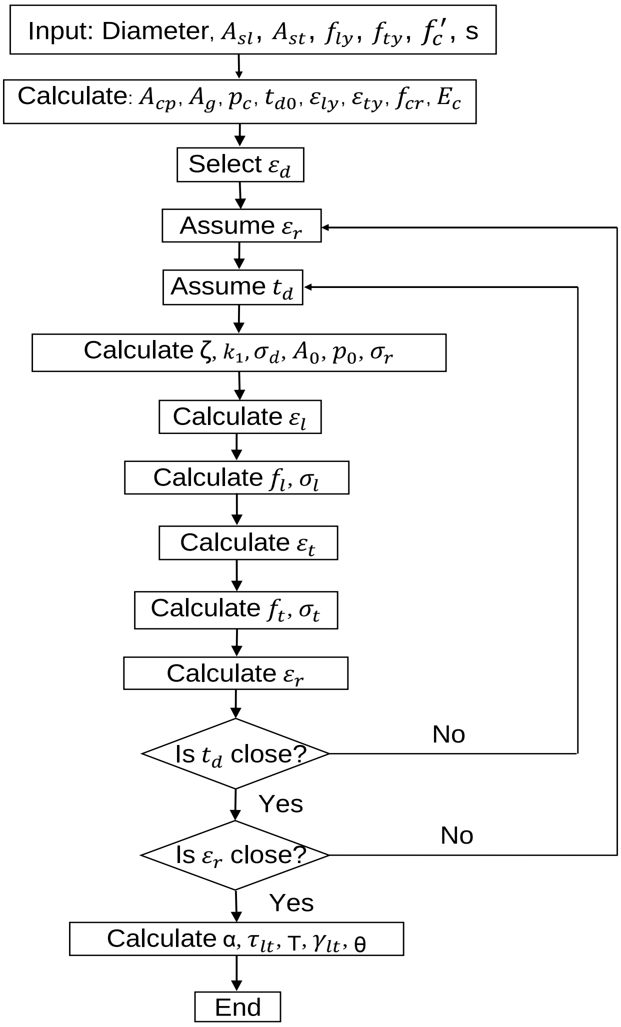

Fig. 5 Solution procedure for TS-STM

1. Select a value of ε_d
2. Assume a value of ε_r.
3. Assume a value of t_d.
4. Calculate ζ, k_1, σ_d, A_o and p_o from the corresponding Eqs. (16), (15), (14), (23), (24). Before cracking, calculate σ_r using 17. After cracking, use the tension stiffening model to calculate σ_r using Eqs. (18a), (18b), (18c) respectively.
5. Calculate ε_l using Eq. (25).
6. Calculate ε_t using Eq. (26).
7. Calculate ε_r from Eq. (27). If the difference between the assumed and calculated value of ε_r is not within a tolerable limit, then repeat Steps 2 to 6 until the convergence is achieved.
8. Calculate α, τ_{lt}, T, γ_{lt} and θ using Eqs. (28), (4), (6), (9) and (10) respectively, corresponding to one value of ε_d.
9. Repeat the process for different values of ε_d.

5. Experimental corroboration of proposed model

The proposed TS-STM was validated through comparison with test data on RC square columns tested under torsional loading. Experimental results obtained from two specimens (TP-91 and TP-92) tested in the University of Tokyo and one specimen (Missouri) tested in the University of Missouri were used for calibration purpose. The details of the test setup and loading protocol can be found in Tirasit and Kawasima (2007a, b), Prakash (2009), Prakash *et al*. (2012). Predictions were made using the linear, parabolic, and exponential models of tension stiffening. The cracking and peak values of torque and twist obtained from the analytical and experimental results, on comparison, yielded an appreciable correlation. The observed errors may be attributed to material imperfections or the discrepancy in loading steps. The details of the test specimens are summarised in Table 3 and the reinforcement detailing is shown in Fig. 6.

Table 3 Specimen details

Specimen Id	**TP-91**	**TP-92**	**Missouri**
Section Shape	Square	Square	Square
Section Dimension (m×m)	0.40×0.40	0.40×0.40	0.56×0.56
Column Height (m)	1.75	1.75	3.35
Cylinder Strength of Concrete (MPa)	28.3	28.4	34.6
Longitudinal Reinforcement Ratio (%)	1.27	1.27	2.10
Transverse Reinforcement Ratio (%)	0.75	0.75	1.32
Longitudinal Reinforcement Yield Strength (MPa)	354	354	512
Transverse Reinforcement Yield Strength (MPa)	328	328	454
Axial Force (kN)	0	160	0
Young's Modulus of Steel (MPa)	200000	200000	200000

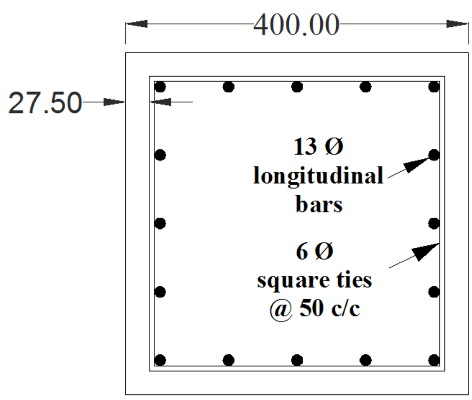

(a) TP-91 and TP-92

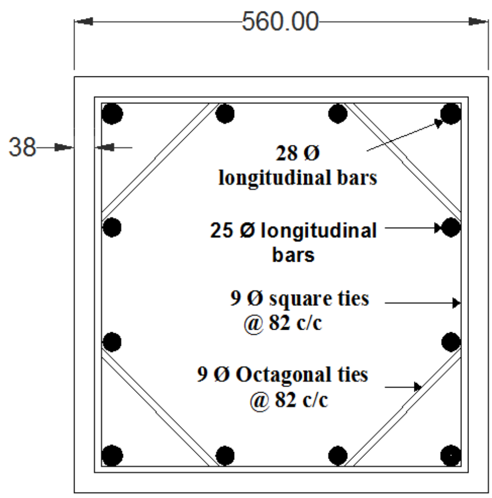

(b) Missouri

Fig. 6 Reinforcement detailing of the test specimens (dimensions in mm)

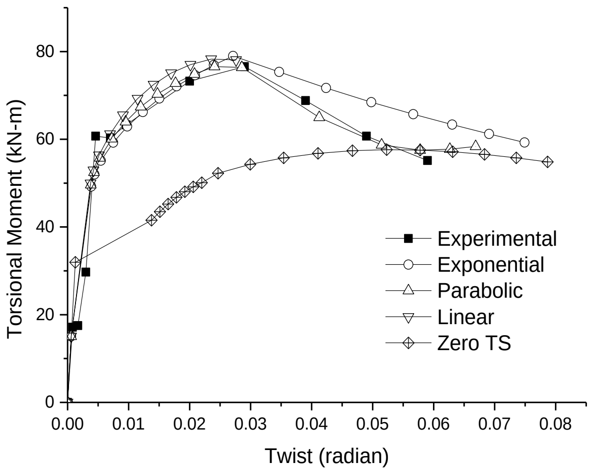

(a) Test specimen TP-91

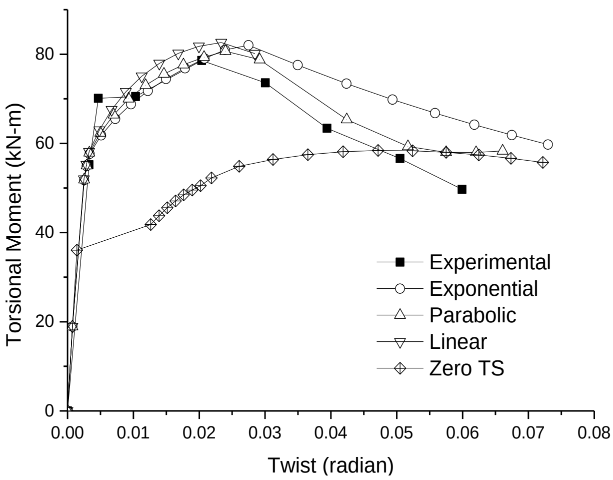

(b)Test specimen TP-92

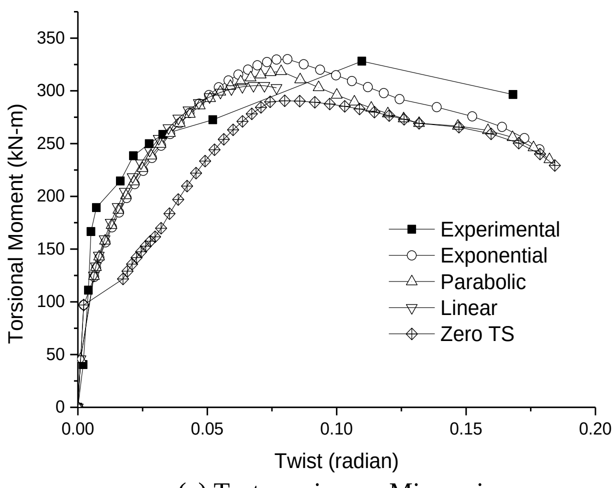

(c) Test specimen - Missouri

Fig. 7 Comparison of efficiency of different TS model in predicting torque-twist behaviour

6. Overall torsional response

The torque-twist behaviour of the tested columns predicted by TS-STM is compared with test data in Fig. 7. It can be observed that the predictions of the three tension stiffening models used in this study are identical up to the peak torque. For larger tensile strains, the tensile stresses predicted by the tension stiffening models are markedly different. So, the predicted torque-twist behaviour is no longer identical. However, the difference is not large, as the effect of tension stiffening is small near and after the peak. The linear model failed to predict the behaviour in post peak region (Fig. 7). The behaviour predicted by the exponential and the parabolic models is close to the experimentally measured values and therefore any of the two models can be used interchangeably to obtain equally valid prediction. However, the torque-twist behaviour predicted by the original STM is initially very stiff up to cracking, followed by a reduced stiffness up to the peak torque, which contrasts sharply with the behaviour predicted by TS-STM. Thus, the original STM is shown to underestimate the stiffness and leads to overestimation of the deformation in post cracking region. The value of peak torque predicted by TS-STM is larger than the peak torque predicted by STM owing to the effect of tension stiffening.

7. Peak response

The values of peak torque and twist for the three columns predicted by the TS-STM are shown in Table 4 and compared with the experimental values. It may be noted that the linear and the parabolic tension stiffening models, on an average, predict the ultimate torque value almost accurately, while the exponential model overestimates the same by 2.67%. On the other hand, the predictions of twist at the peak by the three models were broadly similar. Hence, it may be commented that all the three tension stiffening models predict the behaviour at the peak reasonably well and the predictions are close to experimental observations. On the other hand, the original STM under predicts the peak torsional capacity significantly. Since, for the specimens considered in this study, longitudinal reinforcement ratio was greater than the transverse reinforcement ratio, it is imperative that average strain in longitudinal steel will be less than that in transverse steel. As a result, angle of inclination α will be slightly greater than 45 degree for the specimens under consideration. Now, neglecting tensile stress in concrete (σ_r) (as in original STM) will lead to under prediction of shear stress (τ_{lt}) by $\frac{1}{2}\sigma_r \sin 2\alpha$ (Eq. (4)), which may not be too small to be neglected because of α being close to 45 degree. The discrepancy is amplified when τ_{lt} is multiplied with $2A_0 t_d$ (not a small number) to obtain torsional moment, *T*. This explains the large discrepancy in peak torque values predicted by the proposed TS-STM and the original STM.

8. Strains in longitudinal and transverse reinforcements

Fig. 8 shows the variation in strain in the longitudinal and the transverse reinforcements with applied torque for test specimen TP-92. The predictions of all the three tension stiffening models closely follow the experimental measurements up to the peak torque. The behaviour shows an initial steep slope as torque increases without significant increase in stress in the reinforcements. This is due to the shear flow in concrete resisting most of the applied torque. The response is effectively linear before cracking and subsequently it flattens out. The strain in both kinds of reinforcement is tensile bringing about an apparent truss action. Further, it may be inferred from the figure that the exponential model mimics the variation in strain in the longitudinal reinforcements with applied torque in a better way than the remaining two models whereas the same in the transverse reinforcements can be best represented by the parabolic model. The linear model produced no result in the post peak region as mentioned above.

It is observed in Fig. 8 that the transverse reinforcement reached the yield point much before the failure of the specimens. On the other hand, the maximum strain in the longitudinal reinforcement at failure was less than the yield strain. This may be attributed to higher ratio of longitudinal reinforcement than that of transverse reinforcement (Table 3) used in the specimens.

Table 4 Ultimate torque and twist

Specimen Name	Parameter	Experimental	Linear Model	Parabolic Model	Exponential Model	Zero Tension Stiffening Case
TP-91	T_u (Kn-m)	76.57	78.28	76.57	78.99	57.39
	θ_u (rad)	0.029	0.028	0.029	0.027	0.047
	$T_{u,calc} / T_{u,test}$	NA	1.02	1.00	1.03	0.75
	$\theta_{u,calc} / \theta_{u,test}$	NA	0.97	1.00	0.93	1.61
TP-92	T_u (Kn-m)	78.59	82.62	80.70	82.01	57.46
	θ_u (rad)	0.020	0.023	0.024	0.027	0.037
	$T_{u,calc} / T_{u,test}$	NA	1.05	1.03	1.04	0.73
	$\theta_{u,calc} / \theta_{u,test}$	NA	1.15	1.2	1.35	1.79
Missouri	T_u (Kn-m)	328.09	304.92	318.49	330.04	290.59
	θ_u (rad)	0.110	0.072	0.079	0.081	0.080
	$T_{u,calc} / T_{u,test}$	NA	0.93	0.97	1.01	0.89
	$\theta_{u,calc} / \theta_{u,test}$	NA	0.65	0.72	0.74	0.73

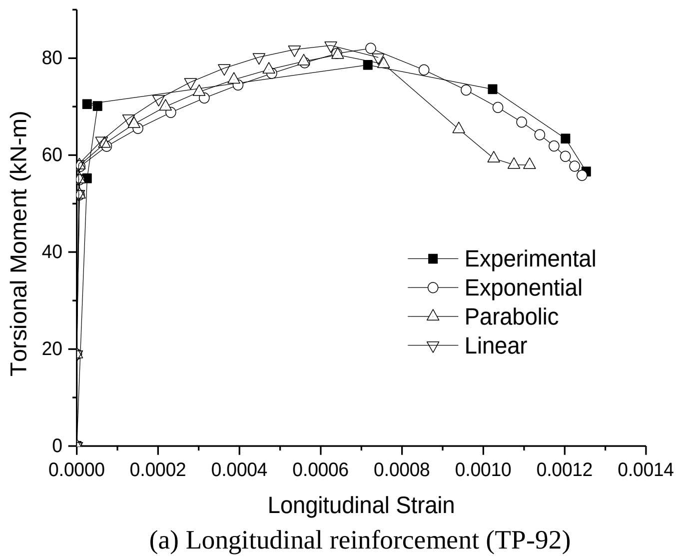

(a) Longitudinal reinforcement (TP-92)

Fig. 8 Comparison of efficiency of different TS model in predicting average strain in reinforcements

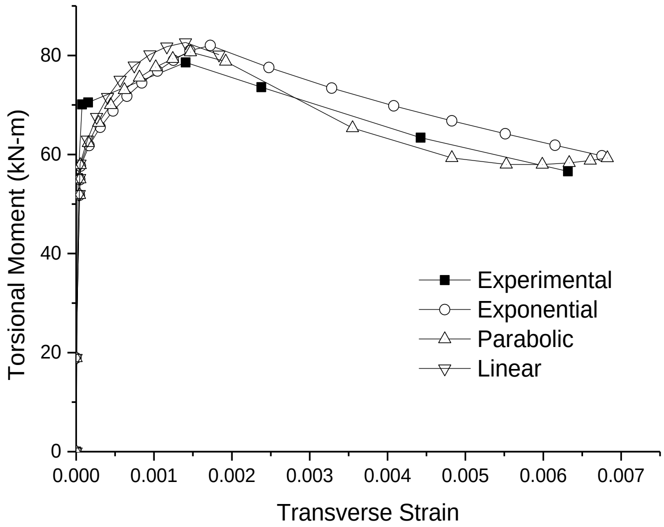

(b) Transverse reinforcement (TP-92)

Fig. 8 Continued

As proposed by Leu and Lee (2000), reinforced concrete sections can be classified into four categories based on relative percentage of longitudinal and transverse steel. For large ratio of longitudinal and transverse steel, concrete fails in compression before any of the reinforcements reaches the yield stress. Such sections are referred to as over reinforced sections. The condition under which both the reinforcing steels reach yield stress simultaneously with concrete reaching ultimate strain in compression is known as balanced condition. If the longitudinal and transverse reinforcement ratios are less than that corresponding to balanced condition, then the reinforcements reach yield condition before crushing of concrete in compression. Such failure mode is called as under reinforced failure mode. If any one of the two reinforcement ratios is lower than that for balanced condition, then either the longitudinal or the transverse reinforcement yields before the concrete is crushed. Such type of sections is termed as partially under reinforced sections. The specimens considered in the present study are typical examples of partially under reinforced section where the concrete crushes prior to the yield of longitudinal reinforcement and after the yield of transverse reinforcement. Therefore, the sections are under reinforced in transverse direction and over reinforced in longitudinal direction.

9. Conclusions

The proposed model includes the effect of concrete tension stiffening to provide a continuous prediction of torsional behaviour of square RC columns before and after cracking. In this model, the alignment of cracks rotate to remain normal to the principal tensile stress and the contribution of concrete in shear is neglected. The model assumes perfect bond between the concrete and reinforcement. The model has been validated by comparing the predicted and experimental behaviour of members loaded under torsion with or without axial compression.

The following conclusions can be arrived from the improved TS-STM developed in this study:

• Comparison of predictions with experimental data shows that tension stiffening has a significant influence in the torque-twist response of an RC square member and it has to be considered in the design criteria.

• The concept of an apparent truss model was adopted to justify the prediction of an uncracked member under torsion using a truss model. This resulted in closer predictions both in the pre-cracking and post-cracking region.

• Test specimens used for the validation of the models had the following failure progression: shear cracking, transverse reinforcement yielding and diagonal compression failure of concrete. This failure progression was adequately captured by the developed TS-STM.

• The torque-twist behaviour and reinforcement strains predicted by the TS-STM was compared to test results and showed a close comparison.

• Linear, parabolic, and exponential models of concrete tension stiffening produced fairly close predictions before the peak torque. The parabolic and the exponential models have comparable capacity to model the torsional behaviour in the post peak region. The linear model proved inefficient in the post peak region.

Acknowledgements

This analytical work is carried out as part of a project funded by SERB, Department of Science and Technology, India. Their financial support is gratefully acknowledged. Part of the experimental data used in this study was obtained from tests carried out as a part of a project funded by NEES-NSF-NEESR, USA, and the National University Transportation Centre, and the Intelligent Systems Centre of Missouri S&T, USA. Their financial support during the PhD work of second author is gratefully acknowledged. The authors would also like to thank Professor K. Kawashima (University of Tokyo) and his team for sharing the test data on RC square columns subjected to torsional loading.

References

ACI (American Concrete Institute) (2005), ACI 318-08: Building Code Requirements for Reinforced Concrete and Commentary, American Concrete Institute, Detroit, MI, USA.

Belarbi, A. and Hsu, T.T.C. (1994), "Constitutive laws of concrete in tension and reinforcing bars stiffened by concrete", *ACI Struct. J.*, **91**(4), 465-474.

Bredt, R. (1896), "Kritische Bemerkungen zur Drehungselastizitat", *Zeitschrift des Vereines Deutscher Ingenieure*, Band 40, No. 28, No. 29, 813-817.

Choi, C.K. and Cheung, S.H. (1996), "Tension stiffening model for planar reinforced concrete members", *Comput. Struct.*, **59**, 179-190.

Collins, M.P. and Mitchell, D. (1991), *Prestressed Concrete Structures*, Response Publications, Canada.

Elenas, A., Vasilidis, L., Pouliou, E. and Emmanouilidou, N. (2006), *Influence of Tension Stiffening Effect on Design and Behaviour of Reinforced Concrete Structures*, Measuring, Monitoring and Modelling Concrete Properties, An International Symposium dedicated to Professor SP. Shah, Springer.

Greene, G.G. (2006), "Behaviour *of* reinforced concrete girders under cyclic torsion and torsion combined with shear: experimental investigation and analytical models", Ph.D. Thesis, Department of Civil, Architectural, and Environmental Engineering, University of Missouri at Rolla, Rolla, USA.

Hsu, T.T.C. and Mo, Y.L. (1985a), "Softening of concrete in torsional members-theory and tests", *J. Am.*

Concrete Ins. Pr., **82**(3), 290-303.
Hsu, T.T.C. (1988), "Softened truss model theory for shear and torsion", *ACI Struct. J.*, 85-56.
Hsu, T.T.C. (1991), "Nonlinear analysis of concrete torsional members", *ACI Struct. J.*, 88-69.
Hsu, T.T.C. (1993), *Unified Theory of Reinforced Concrete*, Library of Congress Cataloging, C.R.C. Press, 257-287.
Leu, L.J. and Lee, Y.S. (2000), "Torsion design charts for reinforced concrete rectangular members," *J. Struct. Eng.*, ASCE, **126**(2), 210-218.
Mondal, T.G. and Prakash, S.S. (2015), "Effect of tension stiffening on the behaviour of reinforced concrete circular columns under torsion", *Eng. Struct.*, **92**(1), 186-195.
Prakash, S. (2009), "Seismic behavior of RC circular columns under combined loading including torsion", Department of Civil Engineering, Missouri University of Science and Technology, Missouri, USA.
Prakash, S., Li, Q. and Belarbi, A. (2012), "Behaviour of circular and square reinforced concrete bridge columns under combined loading including torsion", *ACI Struct. J.*, **109**(3), 317-328.
Stramandinoli, R. S. B. and Rovere, H. L. L. (2008), "An efficient tension stiffening model for nonlinear analysis of reinforced concrete members", *Eng. Struct.*, **30**, 2069-2080.
Stevens, N.J., Uzumeri, S.M. and Collins, M.P. (1987), "Analytical modelling of reinforced concrete subjected to monotonic and reversed loadings", Department of Civil Engineering, University of Toronto, Canada.
Tirasit, P. and Kawashima, K. (2007a), "Seismic performance of square reinforced concrete columns under combined cyclic flexural and torsional loadings", *J. Earthq. Eng.*, **11**, 425-452.
Tirasit, P. and Kawashima, K. (2007b), "Effect of nonlinear torsion on the performance of skewed bridge piers", *J. Earthq. Eng.*, **12**, 980-998.
Vecchio, F.J. and Collins, M.P. (1981), "Stress-strain characteristic of reinforced concrete in pure shear", IABSE Colloquium, Advanced Mechanics of Reinforced Concrete, Delft, Final Repo International Association of Bridge and Structural Engineering, Zurich, Switzerland.
Vecchio, F.J. and Collins, M. (1986), "The modified compression-field theory for reinforced concrete elements subjected to shear", *ACI Struct. J.*, **83**(2), 219-231.
You, Y.M. and Belarbi, A. (2011), "Thickness of shear flow zone in a circular column under pure torsion", *Eng. Struct.*, **33**, 2435-2447.

PL

Notations

t_d Thickness of shear flow zone
t_{d0} Thickness of shear flow zone at cracking.
p_c Perimeter of the column section
s Spacing between adjacent transverse reinforcements
A_{cp} Area bounded by p_c
ε_l Average longitudinal strain
ε_t Average transverse strain
γ_{lt} Average shear strain in *l*-*t* plane
σ_l Average normal stress in longitudinal direction
σ_t Average normal stress in transverse direction
τ_{lt} Average shear stress in *l*-*t* plane
σ_d Average concrete compressive stress

ε_d	Average concrete compressive strain
f'_c	Peak compressive stress of concrete
ε_0	Strain in concrete at fc’
ζ	Softening coefficient of concrete
ε_r	Average tensile strain in concrete
σ_r	Average tensile stress in concrete
f_{cr}	Cracking strength of concrete
ε_{cr}	Cracking strain of concrete
ε_l	Average strain in longitudinal steel
f_l	Average stress in longitudinal steel
ε_t	Average strain in transverse steel
f_t	Average stress in transverse steel
ε_y	Yield strain of steel
f_y	Yield stress of steel
ρ_l	Volumetric ratio of longitudinal steel
ρ_t	Volumetric ratio of transverse steel
ψ	Curvature in the concrete strut
E_c	Modulus of elasticity of concrete
f_{ck}	Characteristic compressive strength of concrete
γ	Poisson’s ratio of concrete
G	Modulus of rigidity of concrete
K	Polar moment of inertia of the section
E_s	Modulus of elasticity of steel
T	Torsional moment
θ	Angle of twist
T_{cr}	Cracking torque
θ_{cr}	Cracking twist